Generation and propagation of high-order harmonics in crystals

Shambhu Ghimire,[1,*] Anthony D. DiChiara,[2] Emily Sistrunk,[2] Georges Ndabashimiye,[1] Urszula B. Szafruga,[2] Anis Mohammad,[3] Pierre Agostini,[2] Louis F. DiMauro,[2] and David A. Reis[1,4,†]

[1]*Stanford PULSE Institute, SLAC National Accelerator Laboratory, Menlo Park, California 94025, USA*

[2]*Physics Department, Ohio State University, Columbus, Ohio 43210, USA*

[3]*The Linac Coherent Light Source, SLAC National Accelerator Laboratory, Menlo Park, California 94025, USA*

[4]*Departments of Photon Science and Applied Physics, Stanford University, Stanford, California 94305, USA*

(Received 9 January 2012; published 20 April 2012)

The observation of nonperturbative high-order-harmonic generation in periodic solids has been interpreted in terms of a two step process comprising tunnel ionization and radiation from electrons undergoing frequency modulated Bloch oscillations in a strong laser field [Ghimire *et al*., Nat. Phys. **7**, 138 (2011)]. Here we extend the model to include propagation effects. We show that the predicted efficiency is limited by phase velocity mismatch for emission below the band gap and by absorption above the band gap. The efficiency of harmonics scales with the square of the carrier density, suggesting that direct seeding could lead to higher yield. The emitted harmonics should have a temporal profile consisting of a train of subcycle pulses with duration on the order of 650 as depending on the crystal thickness.

DOI: 10.1103/PhysRevA.85.043836 PACS number(s): 42.65.Ky, 42.65.Re

High-order-harmonic generation (HHG) in the strong-field limit is the standard route for producing attosecond pulses [1,2]. The typical interaction medium is a dilute atomic gas [3,4] although nonperturbative harmonics have also been produced from molecules [5–7], metal surfaces [8,9], and plasma plumes [10–12]. Recently we reported the first observation of nonperturbative harmonics in a bulk crystal in the strong-field limit using ultrashort midinfrared (MIR) laser pulses centered at 3.25 μm [13]. In these experiments on ZnO, harmonics up to the 25th order were observed in 1 kHz repetition rate without damaging sample for a maximum peak field of 0.6 V/Å—approaching the limit of the band gap per lattice constant, but well below the relativistic limit [14,15].

Bulk crystals have the potential for efficient conversion due to the high density; however, the process cannot simply be seen as the emission from a large number of independent atoms. We expect the mechanism for nonperturbative harmonic generation in periodic solids to be fundamentally different than the atomic case due to the built-in coherence between the multiple and closely spaced sites. The single-atom high-harmonics spectrum cuts off in energy at $I_p + 3.17U_p$, where I_p is the ionization potential of the neutral atom and $U_p = e^2E_0^2/4m\omega^2$ is the ponderomotive energy [16–18]. Gas phase experiments have verified that so long as the ground state is not depleted, the cutoff scales quadratically with both the laser peak field [19] and the wavelength [20,21]. The single atom based picture of HHG is not valid in solids because the excursion amplitude of a free electron in the laser field, ~32 Å for a field of 0.6 V/Å and wavelength of 3.25 μm, is many times the typical nearest neighbor distance. The corresponding ponderomotive energy for a free electron, ~5 eV, also exceeds the typical energy scale of the valence and conduction bands. Thus, for strong field processes such as HHG in solids, the influence of the periodic potential on the electrons cannot be ignored—or even treated in terms of a constant effective mass [22]. One important way the periodic potential manifests itself is in the linear scaling of the high-energy cutoff of the HHG with field [13]. It has also been predicted that the HHG spectrum would have an imprint of the electronic states in solids [13,23,24].

The general features of the harmonic emission observed by Ghimire *et al*. [13] are accommodated by a simple two-step model comprising tunneling between valence and conduction bands, and the radiation from a nonlinear intraband current. In this model, the nonlinearity is due to a combination of anharmonic electron motion in the band along with the multiple Bragg reflections at the zone boundaries—which repeats every half cycle of the laser field and radiates odd multiples of the drive laser frequency (i.e., frequency modulated Bloch oscillations [25,26]). Here we discuss where the fundamental differences in the generation processes arise and include one-dimensional propagation effects that allows us to calculate the efficiency for any given harmonic order in terms of a nonlinear conductivity. We discuss possible routes to higher efficiency and their limitations, and we show that because the harmonics are phase locked, attosecond pulse trains and perhaps even isolated attosecond pulses can be generated.

As in [13], we treat the nonperturbative high-order-harmonic generation in crystals in the strong-field limit in a two-step model as illustrated in Fig. 1(a): (i) ionization—a small fraction of electrons tunnel from a previously occupied valence band to an unoccupied conduction band close to zone center near the peak of the linearly polarized field; and (ii) intraband acceleration—the strong field drives the electrons (and holes [27]) in the band producing a nonlinear current that subsequently radiate nonperturbative harmonics. We neglect stimulated emission and nonlinear Rabi oscillations [28–30] and assume that the harmonics are entirely due to the intraband current. The tunneling step therefore serves to

*shambhu@slac.stanford.edu
†dreis@slac.stanford.edu

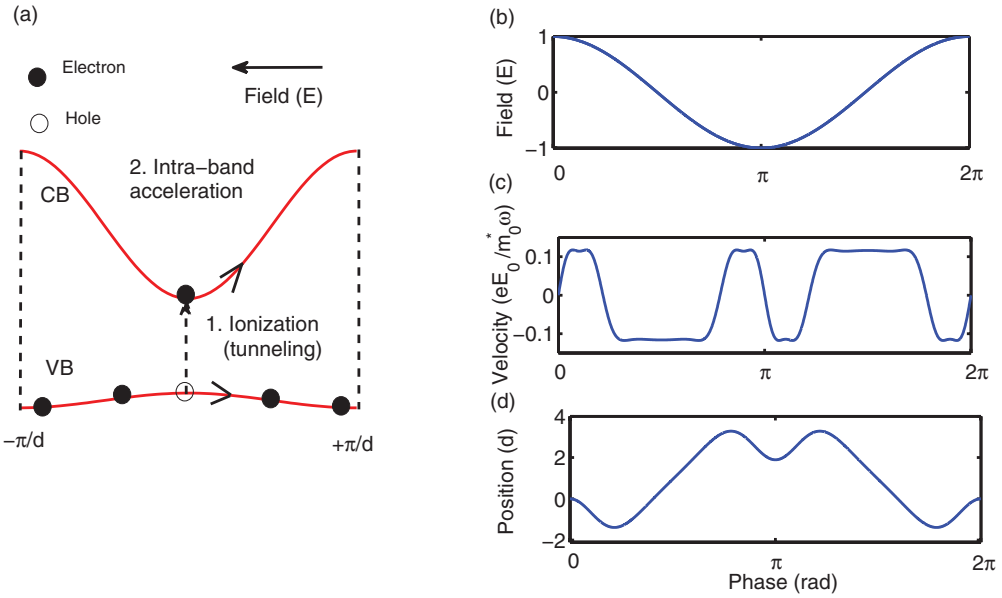

FIG. 1. (Color online) (a) Schematic of the band model for two step high-order-harmonic generation in the strong-field limit. In the first step a small fraction electrons from the valence band tunnel to the conduction band near zone center at the peaks of the electric field [shown in (b)]. In the second step the carriers undergo nonlinear acceleration within the band which radiates harmonics for a periodic drive. The corresponding velocity (c) of the electron wave packet and trajectory (d) in units of $eE_0/m^*\omega$ and lattice spacing d, respectively, for parameters given in Ref. [13].

seed carriers to the conduction band near the peak of the field.

Consider first the semiclassical motion of a single electron wave packet in a cosine band

$$\epsilon(q) = \frac{\hbar^2}{m_0^* d^2}[1 - \cos(qd)], \tag{1}$$

where m_0^* is the band effective mass at zone center and d is the lattice spacing. In the presence of a strong harmonically varying laser field $E(t) = E_0 \cos(kz - \omega t)$ propagating along the z axis, the electron wave vector (relative to its value at $t = 0$),

$$q(t) = -\frac{e}{\hbar}\int_0^t E(t')dt' = \frac{eE_0}{\hbar\omega}\sin(kz - \omega t) + q(0). \tag{2}$$

Thus, the group velocity,

$$v_g = \frac{1}{\hbar}\frac{\partial\epsilon(q)}{\partial q} = \frac{\hbar}{m_0^* d}\sin\left[\frac{\omega_B}{\omega}\sin(kz - \omega t) + q(0)\right], \tag{3}$$

where $\omega_B = eE_0 d/\hbar$ is the Bloch frequency corresponding to the peak field (i.e., the rate at which electrons traverse the Brillouin zone in a dc field in the absence of scattering).

The group velocity is time varying and anharmonic, exhibiting frequency components at odd harmonics of the fundamental. This is made explicit when we recast (3) in terms of its Bessel function (Jacobi-Anger) expansion, which for $q(0) = 0$ is

$$v_g = \frac{eE_0}{m_0^*\omega}\sum_{s=1}^{\infty}\frac{1}{2s-1}\left[J_{2s-2}\left(\frac{\omega_B}{\omega}\right) + J_{2s}\left(\frac{\omega_B}{\omega}\right)\right] \times \sin[(2s-1)(kz - \omega t)]. \tag{4}$$

Equation (4) reduces to the perturbative limit when $\omega_B \ll \omega$, where the electrons make small oscillations about the zone center. Here the anharmonic terms in the group velocity are due to the finite dispersion in the effective mass, that is, the nonparabolicity of the band. For higher fields the oscillations are no longer small compared to the length of the Brillouin zone and the dispersion can become substantial. For high enough fields, that is, $\omega_B \gtrsim 2\omega$, the electrons traverse the entire Brillouin zone and undergo periodic Bragg scattering at the zone boundaries within a half laser cycle. Here the frequency content scales nonperturbatively, extending to roughly $(2s-1)\omega = \omega_B$, after which it drops rapidly with increasing order. Thus we see that in the high-field limit, the high-energy cutoff is linearly proportional to the electric field and effectively independent of drive frequency.

The above results can be extended for an arbitrary band. We write the electronic band dispersion in terms of the Fourier expansion of the direct lattice [31], $\epsilon(q) = c_0/2 + \sum_{p=1}^{\infty} c_p \cos(pqd)$. In this case the general form of group velocity,

$$v_g = \frac{eE_0}{m_0^*\omega}\sum_{p,s=1}^{\infty}\frac{p^2 b_p}{2s-1}\left[J_{2s-2}\left(p\frac{\omega_B}{\omega}\right) + J_{2s}\left(p\frac{\omega_B}{\omega}\right)\right] \times \sin[(2s-1)(kz - \omega t)], \tag{5}$$

where $b_p = c_p/\sum p^2 c_p = c_p d^2 m_0^*/\hbar^2$ are scaled Fourier coefficients [13]. The main difference is that the additional dispersion in the effective mass leads to higher frequency content than in a purely cosine band, extending the cutoff to an integer number of the Bloch frequency depending on the steepness of the band. As was done in Ref. [13], we take $\omega_B = 5\omega$ and dispersion $[\epsilon(q) = 2.5(1 - 0.95\cos qd - 0.05\cos 3qd)$ (eV)], where $d = \sqrt{3}a/2 \approx 2.8$ Å which approximates the first conduction band of ZnO along **Γ**-**M** [32].The group velocity at $z = 0$ is plotted in Fig. 1(c) for normalized field in Fig. 1(b). Note that the higher frequency components occur near the peak

of the field where the effects of both the Bragg scattering and the high-spatial harmonics of the band can be seen clearly.

The trajectory of an electron wave packet which is initially at q and $t = 0$ is given by

$$x(t,z) = \frac{eE_0}{m_0^*\omega^2}\sum_{p,s=1}^{\infty}\frac{p^2 b_p}{(2s-1)^2}\left[J_{2s-2}\left(p\frac{\omega_B}{\omega}\right)+J_{2s}\left(p\frac{\omega_B}{\omega}\right)\right] \times\{1-\cos[(2s-1)(kz-\omega t)]\}. \quad (6)$$

We plot the trajectory in Fig. 1(d) in the units of nearest neighbor distance d. The effect of the Bragg scattering on the trajectory is to localize the electron wave packet [33]. In contrast to the atomic case where the maximum excursion increases with the field, in the periodic solid, the electron wave packet becomes more localized about the cores with increasing field once $\omega_B \gtrsim \omega$. In the atomic case the further the electron is accelerated from the core, the more energy it gains in the field such that the ponderomotive energy is proportional to the square of the electric field and inversely with the square of the drive frequency. For solids in low peak fields, the effective mass approximation may be appropriate and the ponderomotive energy of an electron in the band can be considered to be $U_p^* = e^2E^2/4m_0^*\omega^2$, analogous to the atomic case. However, for high enough fields where the dispersion in the effective mass becomes appreciable, the ponderomotive energy deviates from the quadratic dependence with field, showing oscillatory behavior confined by the electronic bandwidth [34].

In order to calculate the efficiency of the harmonic generation, we consider the total electric field (in complex notation) as $E(z,t) = \sum_{s=1}^{\infty} E_{2s-1}(z)e^{i(k_{2s-1}z-\omega_{2s-1}t)}$, with $\omega_{2s-1} = (2s-1)\omega$ and look for solutions to the one-dimensional coupled wave equations [35],

$$\frac{\partial^2 E_{2s-1}}{\partial z^2} - \mu_0\epsilon_0[1+\chi(\omega_{2s-1})]\frac{\partial^2 E_{2s-1}}{\partial t^2} = \mu_0\frac{\partial j_{2s-1}}{\partial t}. \quad (7)$$

We treat the nonlinearity only in the intraband current and assume that higher orders of the polarizability can be neglected. This is reasonable when the drive photon energy is well below the gap (approximately nine photons in Ref. [13]). To leading order, this means that we ignore "$\chi^{(3)}$" processes such as self-phase modulation and self-focusing. These effects are mitigated in the experiment by tight focusing of the drive laser on the exit of the crystal. Because the interaction length turns out to be small compared to the Rayleigh range, we consider only one-dimensional propagation. The nonlinear current density in (7) provides the source of the harmonics. For simplicity we assume a steady-state carrier density N. We can then write the $(2s-1)$th component of the current as

$$j_{2s-1}(t) = Nev_{g,2s-1} \equiv \tilde{\sigma}_{2s-1}E_1(z)e^{i(2s-1)(kz-\omega t)}, \quad (8)$$

which is accurate to second order in the width of how the carriers are distributed about the zone center, near the peak of the field. Thus from (5), the $(2s-1)$th component of the (complex) conductivity is

$$\tilde{\sigma}_{2s-1}(\omega,\omega_B) = -\frac{Ne^2}{im_0^*(2s-1)\omega}\sum_{p=1}^{\infty}p^2 b_p \times\left[J_{2s-2}\left(p\frac{\omega_B}{\omega}\right)+J_{2s}\left(p\frac{\omega_B}{\omega}\right)\right], \quad (9)$$

where we have neglected the additional contribution of the current from the harmonics acting back on the carriers. In the limit that there is no depletion of the pump $E_1(z) = E_0$ and for slowly varying amplitudes such that $|\frac{\partial^2 E_{2s-1}}{\partial z^2}| \ll |k_{2s-1}\frac{\partial E_{2s-1}}{\partial z}|$,

$$\frac{\partial E_{2s-1}}{\partial z} = -\frac{\mu_0\tilde{\sigma}_{2s-1}\omega_{2s-1}}{2k_{2s-1}}E_0 e^{i\Delta k_{2s-1}z}\ (s\geqslant 2), \quad (10)$$

where we define $\Delta k_{2s-1} = (2s-1)k - k_{2s-1}$. After integration we find

$$\frac{E_{2s-1}}{E_0} = -\frac{\mu_0\tilde{\sigma}_{2s-1}\omega_{2s-1}}{2k_{2s-1}i\Delta k_{2s-1}}(e^{i\Delta k_{2s-1}z}-1)\ (s\geqslant 2). \quad (11)$$

Thus the efficiency of the $(2s-1)$th harmonic is

$$\frac{I_{2s-1}}{I_1} = -\frac{\mu_0^2\tilde{\sigma}_{2s-1}^2c^2\lambda^2}{16\pi^2(2s-1)^2|n_{2s-1}|^2|\Delta n_{2s-1}|^2} \times\left|e^{i\frac{2\pi(2s-1)}{\lambda}\Delta n_{2s-1}z}-1\right|^2, \quad (12)$$

where $n_{2s-1} = \sqrt{1+\chi(\omega_{2s-1})}$ is the complex index of refraction at frequency $(2s-1)\omega$ and $\Delta n_{2s-1} = n_1 - n_{2s-1}$, which is effectively independent of the carrier density when the drive frequency is much greater than the plasma frequency.

In what follows, we consider the case of ZnO with laser parameters as in [13], $\lambda = 3.25\ \mu$m, $\omega_B = 5\omega$, and a 500 μm thick crystal. We assume a modest carrier density of $N = 1\times10^{19}$ cm^{-3}, such that the laser frequency is well above the plasma frequency. The index of refraction was estimated from Ref. [36] for energies below 5 eV and from Ref. [37] for energies above 5 eV. The nonlinear conductivity $\sigma_{2s-1} = \mathrm{Re}\{\tilde{\sigma}_{2s-1}\}$, as calculated by (9), is reproduced in Fig. 2(a). Figure 2(b) shows the calculated efficiency for these conditions. Similar to the conductivity, the efficiency shows multiple plateaus and a high-energy cutoff corresponding to $3\omega_B$ (due to the particular choice of dispersion). The large efficiency of the third harmonic is due in part to the very small phase mismatch well below the gap, and suggests that for high enough carrier density depletion could become important. Because the conductivity scales as the inverse of the harmonic energy, we see from (9) and (12) that in the nonperturbative limit the efficiency at fixed photon energy (and thus the cutoff energy) is effectively independent of the drive wavelength. In contrast, for the atomic case the cutoff energy is quadratic with the wavelength, but the single atom efficiency is dramatically reduced due to diffraction (spreading) of the returning wave packet [20,21,38].

The harmonic emission is limited by absorption above the gap and phase mismatch below the gap, such that the effective generation length is much less than the crystal thickness in Ref. [13]. Figure 3(a) shows the calculated efficiency as a function of crystal thickness for the 5th harmonic, which is well below the gap. Here it is the phase mismatch between the harmonic and the fundamental that limits the efficiency. In this case, the coherence length is approximately 8 μm. Figure 3(b) shows the larger phase mismatch for the 7th harmonic with coherence length approximately 3 μm. In this case, the finite absorption just below the gap limits the efficiency after a couple coherence lengths. Above the band gap, the efficiency (12) is

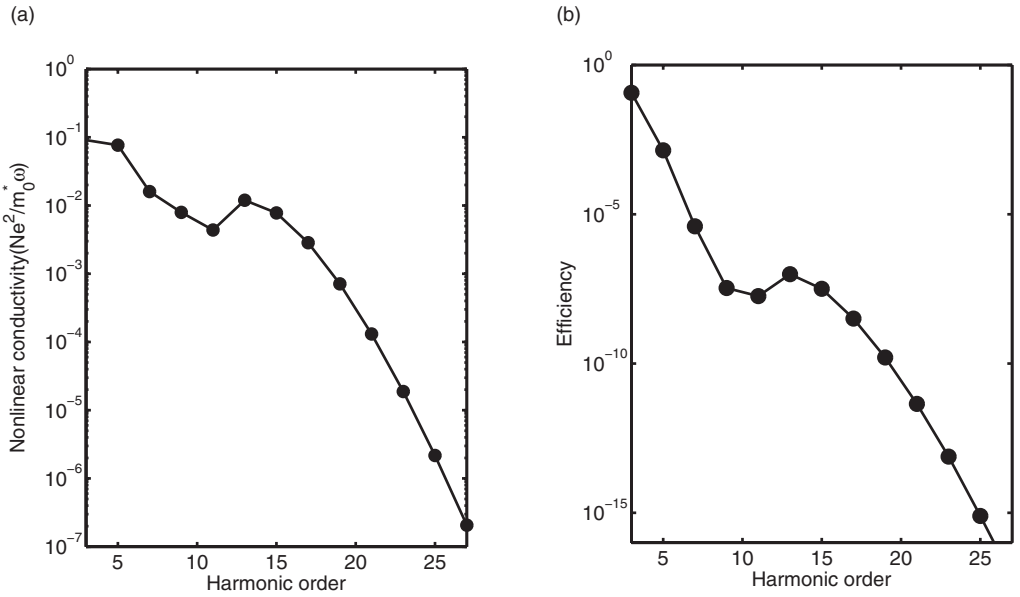

FIG. 2. (a) Calculated nonlinear conductivity for ZnO for band dispersion given in the text for $\omega_B = 5\omega$ in units of $(Ne^2/m_0^*\omega)$. (b) Corresponding efficiency for the high-order harmonics calculated for a 500 μm crystal driven at 3.25 μm fundamental and a carrier density $N = 1 \times 10^{19}$ cm^{-3}.

effectively limited by absorption,

$$\frac{I_{2s-1}}{I_1} = -\frac{\mu_0^2 \sigma_{2s-1}^2 c^2 \lambda^2}{16\pi^2 (2s-1)^2 |n_{2s-1}|^2 \left|\Delta n_{2s-1}^2\right|} \tag{13}$$

as seen in Figs. 3(c) and 3(d) for the 15th and the 21st harmonics, respectively. In addition, because the 21st harmonic falls above the upper cutoff, the efficiency drops dramatically compared to the 15th which is in the upper plateau region as shown in Fig. 2. While the propagation of the below band gap harmonics is modulated mainly by the coherence length the above band gap harmonics are absorption limited, the later could be produced only near the exit face in case of a relatively thick crystal, such as in [13]. We do not consider below gap absorption due to photon assisted tunneling which will reduce the efficiency for the harmonics just below the band gap [22].

Because the harmonics are phase locked, there is the potential for generating ultrashort pulses. In Fig. 4(a) we plot the expected temporal profile and the propagation of

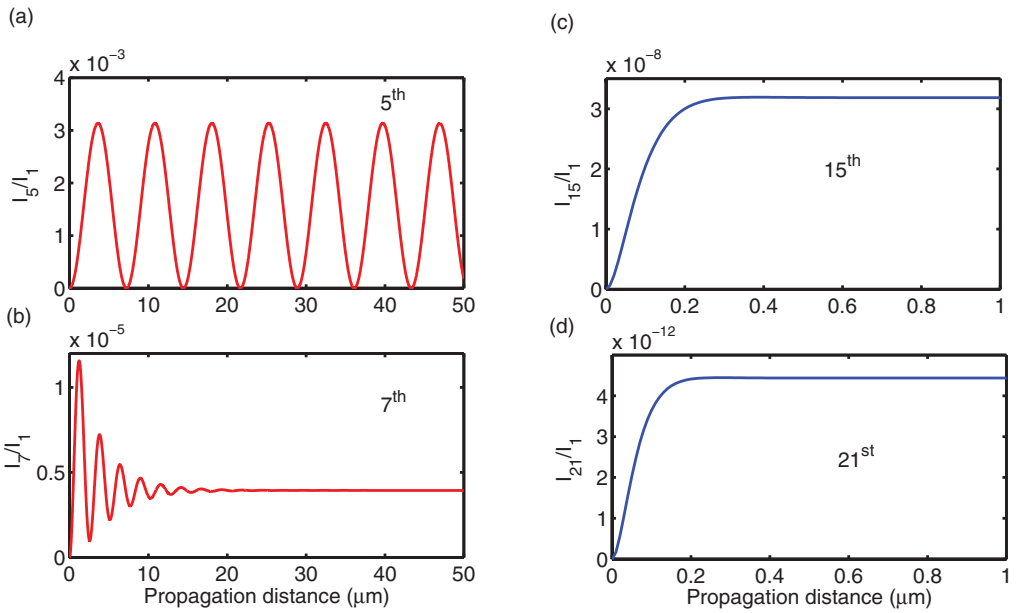

FIG. 3. (Color online) Calculated efficiency as a function of crystal thickness. (a) 5th and (b) 7th are below band gap and the (c) 15th and (d) 21st are above band gap harmonics.

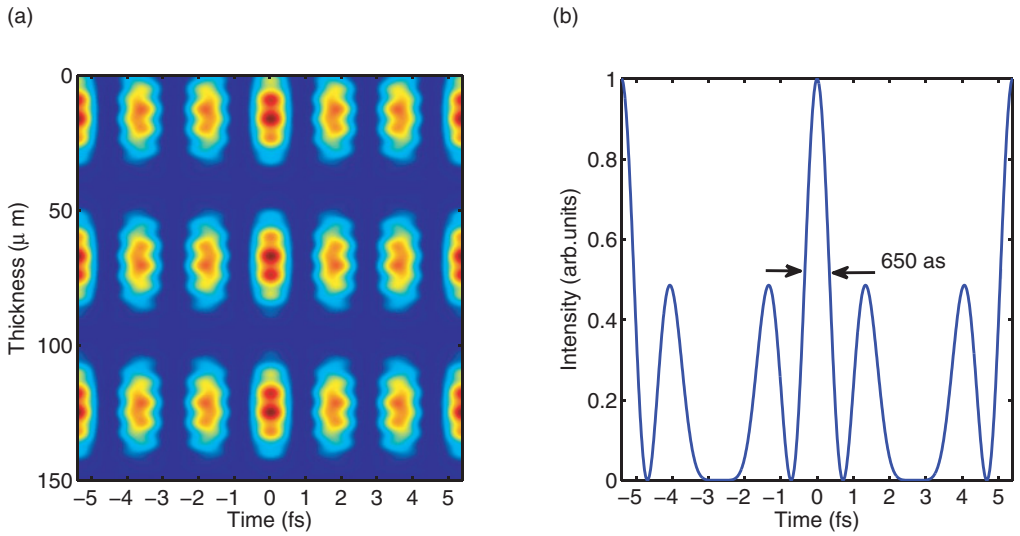

FIG. 4. (Color online) (a) Temporal profile of the harmonics as a function of propagation inside a 150 μm thick crystal which is dominated by the below gap harmonics. (b) A lineout showing an attosecond pulse train at the exit of a 1 μm thick crystal.

high-order harmonics inside a 150 μm thick ZnO crystal. The modulation along the direction of crystal thickness, in about 55 μm, is due to the phase mismatch primarily between the drive laser and third harmonic. The temporal profile of harmonics is a train of attosecond pulses consisting of a main peak every half laser cycle along with side peaks. In Fig. 4(b) we show a lineout of the temporal profile of the harmonics at a crystal thickness of 1 μm. The main peaks have a duration on the order of 650 as. The relative strength of the side peaks with respect to the main peak could be optimized to some extent by effectively changing the thickness of the sample. This may be performed in the experiments by translating the sample with respect to the waist of the laser beam or using a wedged sample. An isolated attosecond pulse may be obtained by using a half cycle driving pulse [39] or by spectrally filtering the near cutoff harmonics in the case of a few cycle driving pulse [1,40]. Alternatively, the generation can be effectively confined to half the laser cycle even in the case of relatively long (many cycle) driving pulses by the method of polarization gating [41,42]. In this method the polarization of the driving pulse is varied, by a set of birefringent wave plates, such that the state of polarization changes rapidly from circular to linear and back to circular, and the width of the linearly polarized portion is controlled by the thickness of the wave plates. In the case of circular polarization the tunneling events are distributed uniformly over the laser cycle, $-\pi > \omega t > +\pi$, unlike the laser phase dependent ionization in a linearly polarized pulse. This corresponds to a lower efficiency in HHG by a factor of $J_0^2(\frac{\omega_B}{\omega})$ compared to the linearly polarized case when propagating along one of the axes of a cubic crystal. The high-energy cutoff also shifts to a lower energy as ω_B is reduced by a factor of $\sqrt{2}$ compared to the case of linear polarization for the same intensity. Additionally, the tunneling rate would be much lower in case of the circular polarization (for the same intensity) which reduces the electron density in the conduction band. This leads to a highly reduced yield in the low orders and no emission in the high orders, consistent with our experimental results [13].

The quadratic dependence on the carrier density could mean that for high enough density the efficiency may be able to exceed the the atomic case. This naturally suggests that the tunneling process be replaced by either doped or metallic samples, or even seeded by photoionization. This has the additional advantage of better control of the process, allowing, for example, the production of efficient circularly polarized harmonics from a circular polarized drive that is otherwise not possible when relying on the tunneling dynamics. Of course at high enough densities, the distribution of the phase of the emission from the individual carriers will result in a reduction in the quadratic growth due to partial destructive interference; however, the efficiency will continue to grow until half filling. Well before this condition is reached, we expect that the drive laser will be reflected from the plasma, at least for crystal thickness large compared to the skin depth. For a cosine band, we find the plasma frequency in the high-field limit is given by

$$\omega_p^2 = \frac{Ne^2}{m_0^*|n_1|^2}\left[J_0\left(\frac{\omega_B}{\omega}\right) + J_2\left(\frac{\omega_B}{\omega}\right)\right], \qquad (14)$$

and the extension to a noncosine band is straightforward. This puts an upper level on the carrier density in Ref. [13] of $N \sim 4 \times 10^{20}$ cm^{-3} (a factor of 40 greater than considered here) given that most of the MIR light is transmitted in those experiments.

In conclusion, we have demonstrated in detail how non-perturbative high-order harmonics could arise in a periodic solid by considering a simple one-dimensional band model. The harmonic generation process is due to the nonlinear acceleration of carriers that tunnel between valence and conduction band in the strong laser field. The process is distinct from the atomic case in that the influence of the (periodic) potential cannot be ignored even as the field approaches the limit of the band gap per lattice constant. The radiation occurs throughout each laser half cycle and could be a new route to attosecond pulse generation. Periodic Bragg scattering (Bloch oscillations) lead to localization of the electron wave packets about the cores and a high-energy cutoff in the radiated

harmonics that scales linearly with field. The efficiency is limited by phase matching below the band gap and by the absorption of harmonics above the band gap. We further show that the efficiency depends on the square of the carrier density suggesting that heavily doped materials or seeding could be a route to higher efficiency, limited by reflection of the pump by the plasma.

ACKNOWLEDGMENTS

S.G., G.N., and D.A.R. acknowledge support by the AMOS program within the Chemical Sciences division of the Office of Basic Energy Sciences, Office of Science, U.S. Department of Energy. The work conducted at OSU is funded by DOE Contracts DE-FG02-06ER15833 and DE-FG02-04ER15614.

[1] M. Drescher *et al.*, Science **291**, 1923 (2001).
[2] P. M. Paul, Science **292**, 1689 (2001).
[3] A. McPherson *et al.*, J. Opt. Soc. Am. B **4**, 595 (1987).
[4] M. Ferray, A. L'Huillier, X. F. Li, L. A. Lomprk, G. Mainfray, and C. Manus, Phys. Rev. Lett. **21**, L31 (1988).
[5] J. Itatani *et al.*, Nature (London) **432**, 867 (2004).
[6] M. Lein, J. Phys. B **40**, R135 (2007).
[7] C. Vozzi, R. Torres, M. Negro, L. Brugnera, T. Siegel, C. Altucci, R. Velotta, F. Frassetto, L. Poletto, P. Villoresi *et al.*, Appl. Phys. Lett. **97**, 241103 (2010).
[8] D. von der Linde, T. Engers, G. Jenke, P. Agostini, G. Grillon, E. Nibbering, A. Mysyrowicz, and A. Antonetti, Phys. Rev. A **52**, R25 (1995).
[9] B. Dromey *et al.*, Nat. Phys. **2**, 456 (2006).
[10] R. Ganeev, M. Suzuki, M. Baba, H. Kuroda, and T. Ozaki, Opt. Lett. **30**, 768 (2005).
[11] R. A. Ganeev, L. B. Elouga Bom, J. Abdul-Hadi, M. C. H. Wong, J. P. Brichta, V. R. Bhardwaj, and T. Ozaki, Phys. Rev. Lett. **102**, 013903 (2009).
[12] R. A. Ganeev, L. B. Elouga Bom, M. C. H. Wong, J.-P. Brichta, V. R. Bhardwaj, P. V. Redkin, and T. Ozaki, Phys. Rev. A **80**, 043808 (2009).
[13] S. Ghimire, A. D. DiChiara, E. Sistrunk, P. Agostini, L. F. DiMauro, and D. A. Reis, Nat. Phys. **7**, 138 (2011).
[14] P. Gibbon, Phys. Rev. Lett. **76**, 50 (1996).
[15] K. Krushelnick, W. Rozmus, U. Wagner, F. N. Beg, S. G. Bochkarev, E. L. Clark, A. E. Dangor, R. G. Evans, A. Gopal, H. Habara *et al.*, Phys. Rev. Lett. **100**, 125005 (2008).
[16] J. L. Krause, K. J. Schafer, and K. C. Kulander, Phys. Rev. Lett. **68**, 3535 (1992).
[17] K. J. Schafer, B. Yang, L. F. DiMauro, and K. C. Kulander, Phys. Rev. Lett. **70**, 1599 (1993).
[18] P. B. Corkum, Phys. Rev. Lett. **71**, 1994 (1993).
[19] B. Shan, S. Ghimire, and Z. Chang, Phys. Rev. A **69**, 021404 (2004).
[20] P. Colosimo *et al.*, Nat. Phys. **4**, 386 (2008).
[21] B. Shan and Z. Chang, Phys. Rev. A **65**, 011804 (2001).
[22] S. Ghimire, A. D. DiChiara, E. Sistrunk, U. B. Szafruga, P. Agostini, L. F. DiMauro, and D. A. Reis, Phys. Rev. Lett. **107**, 167407 (2011).
[23] G. P. Zhang, Phys. Rev. Lett. **95**, 047401 (2005).
[24] G. P. Zhang, D. A. Strubbe, S. G. Louie, and T. F. George, Phys. Rev. A **84**, 023837 (2011).
[25] F. H. M. Faisal and J. Z. Kaminski, Phys. Rev. A **56**, 748 (1997).
[26] D. Golde, T. Meier, and S. W. Koch, Phys. Rev. B **77**, 075330 (2008).
[27] The following arguments apply to the holes as well, but they will generally contribute less to the harmonic generation due to their large effective mass.
[28] B. Sundaram and P. W. Milonni, Phys. Rev. A **41**, 6571 (1990).
[29] O. D. Mücke, T. Tritschler, M. Wegener, U. Morgner, and F. X. Kärtner, Phys. Rev. Lett. **87**, 057401 (2001).
[30] A. Picón, L. Roso, J. Mompart, O. Varela, V. Ahufinger, R. Corbalán, and L. Plaja, Phys. Rev. A **81**, 033420 (2010).
[31] G. Dresselhaus and M. S. Dresselhaus, Phys. Rev. **160**, 649 (1967).
[32] M. Goano, F. Bertazzi, M. Penna, and E. Bellotti, J. Appl. Phys. **102**, 083709 (2007).
[33] D. H. Dunlap and V. M. Kenkre, Phys. Rev. B **34**, 3625 (1986).
[34] V. E. Gruzdev, J. Opt. Technol. **73**, 385 (2006).
[35] J. R. Reitz, *Foundations of Electromagnetic Theory*, 3rd ed. (Narosa Publishing House, Daryaganj, New Delhi, India, 1986).
[36] H. Yoshikawa and S. Adachi, Jpn. J. Appl. Phys. **36**, 6237 (1997).
[37] R. L. Hengehold, R. J. Almassy, and F. L. Pedrotti, Phys. Rev. B **1**, 4784 (1970).
[38] M.-C. Chen, P. Arpin, T. Popmintchev, M. Gerrity, B. Zhang, M. Seaberg, D. Popmintchev, M. M. Murnane, and H. C. Kapteyn, Phys. Rev. Lett. **105**, 173901 (2010).
[39] D. Daranciang, J. Goodfellow, M. Fuchs, H. Wen, S. Ghimire, D. A. Reis, H. Loos, A. S. Fisher, and A. M. Lindenberg, Appl. Phys. Lett. **99**, 141117 (2011).
[40] O. D. Mücke, Phys. Rev. B **84**, 081202 (2011).
[41] G. Sansone *et al.*, Science **314**, 141117 (2006).
[42] B. Shan, S. Ghimire, and Z. Chang, J. Mod. Opt. **52**, 277 (2005).